Penetration of solar radiation in the upper ocean: A numerical model for oceanic and coastal waters

ZhongPing Lee,[1,2] KePing Du,[3] Robert Arnone,[1] SooChin Liew,[4] and Bradley Penta[1]

Received 20 October 2004; revised 11 March 2005; accepted 4 May 2005; published 27 September 2005.

[1] For studies of heat transfer in the upper ocean, the vertical distribution of solar radiation (E_{SR}) in the shortwave domain plays an important role. In earlier studies, a sum of multiple exponentials was used to describe the vertical transmittance of E_{SR}. For those exponential terms, an attenuation coefficient for each term is assigned, and those attenuation coefficients are assumed to be vertically constant. Furthermore, those attenuation coefficients are empirically modeled as functions of chlorophyll concentration (Chl) to cope with varying water properties of the oceans. Since attenuation coefficients of ocean waters are generally determined by components more than Chl alone, we developed a generalized model bypassing the use of Chl on the basis of extensive numerical simulations. In this new model, vertical transmittance of E_{SR} is separated into two exponential terms, with one for the contributions of wavelengths below 700 nm (the visible domain, E_{VIS}) and one for wavelengths above 700 nm (the infrared domain, E_{IR}). An attenuation coefficient is assigned for each of the two exponential terms. Unlike earlier models, these attenuation coefficients vary with depth as expected. Furthermore, the attenuation coefficient for the visible domain is modeled as a function of water's absorption and backscattering coefficients. Since absorption and backscattering coefficients of the world oceans can be adequately derived from observations of ocean color, the model we developed provides an effective and adequate means to describe the three-dimensional variation of both E_{VIS} and E_{SR} in the upper layer of the world oceans.

Citation: Lee, Z., K. Du, R. Arnone, S. Liew, and B. Penta (2005), Penetration of solar radiation in the upper ocean: A numerical model for oceanic and coastal waters, *J. Geophys. Res.*, *110*, C09019, doi:10.1029/2004JC002780.

1. Introduction

[2] For studies of heat transfer in the upper ocean, it is important to reliably provide shortwave solar radiation (E_{SR}, see Table 1 for terms used in this text) in the upper water column [*Zaneveld et al.*, 1981; *Lewis et al.*, 1990]. Knowledge of this vertical distribution of E_{SR} requires information of E_{SR} at the surface and how E_{SR} attenuates with depth (z). The total E_{SR} incident on the water surface can now be estimated with models or measurements made from space [*Gregg and Carder*, 1990; *Mueller et al.*, 2004]. This energy can be considered as two separate portions: energy with wavelengths less than 700 nm (visible domain, E_{VIS}), and energy with wavelengths greater than 700 nm (infrared domain, E_{IR}). The attenuation coefficient for E_{IR} is almost completely dominated by water absorption; thus this attenuation can be viewed as invariable to changes of water constituents [*Morel and Antoine*, 1994]. Also, because of the enormously large absorption coefficients of water molecules, this portion of solar radiation is quickly lost in the upper 3 m [*Morel and Antoine*, 1994].

[3] E_{VIS} encompasses the wavelengths shorter than 700 nm. The pioneer study of *Zaneveld et al.* [1981] and subsequent studies [*Chang and Dickey*, 2004; *Kara et al.*, 2005; *Kirk*, 1988; *Lewis et al.*, 1990; *McClain et al.*, 1996; *Morel and Antoine*, 1994; *Ohlmann et al.*, 2000; *Schneider and Zhu*, 1998; *Siegel et al.*, 1995] have demonstrated that the penetration of E_{VIS} in the upper layer of the ocean plays an important role in heat transfer and sea surface temperature. Unlike the attenuation coefficient for E_{IR}, however, the attenuation coefficient for E_{VIS} changes horizontally with constituents in the water [*Jerlov*, 1976; *Morel and Antoine*, 1994; *Zaneveld et al.*, 1981]. Detailed horizontal information regarding the attenuation coefficient of E_{VIS} is required to determine the global distribution of $E_{VIS}(z)$.

[4] In the past two decades, multiple exponential terms [*Paulson and Simpson*, 1977; *Simpson and Dickey*, 1981; *Zaneveld and Spinrad*, 1980] were generally used to describe the vertical distribution of E_{VIS} or E_{SR} (more reviews can be found in work by *Morel and Antoine* [1994] and *Ohlmann and Siegel* [2000]). For these exponential terms, an attenuation coefficient (or attenuation depth) is assigned for each term. These attenuation coef-

[1]Naval Research Laboratory, Stennis Space Center, Mississippi, USA.
[2]Also visiting professor at Ocean Remote Sensing Institute, Ocean University of China, Qingdao, China.
[3]State Key Laboratory of Remote Sensing Science, Research Center for Remote Sensing and Geographic Information Science, School of Geography, Beijing Normal University, Beijing, China.
[4]Center for Remote Imaging, Sensing and Processing, National University of Singapore, Singapore.

Table 1. Terms and Definitions

	Definition	Units
$a(\lambda)$	absorption coefficient at wavelength λ	m^{-1}
$b_b(\lambda)$	backscattering coefficient at wavelength λ	m^{-1}
Chl	concentration of chlorophyll	mg m^{-3}
$E_d(\lambda, z)$	spectral downwelling irradiance at depth z	W m^{-2} nm^{-1}
$E_{IR}(z)$	downwelling solar radiation for wavelengths in the range of 700–2500 nm, $= \int_{700}^{2500} E_d(\lambda, z)d\lambda$	W m^{-2}
$E_{VIS}(z)$	downwelling solar radiation for wavelengths in the range of 350–700 nm, $= \int_{350}^{700} E_d(\lambda, z)d\lambda$	W m^{-2}
$E_{SR}(z)$	downwelling solar radiation at depth z, $= E_{VIS}(z) + E_{IR}(z)$	W m^{-2}
$K_d(\lambda)$	diffuse attenuation coefficient for $E_d(\lambda, z)$ at λ	m^{-1}
$\hat{K}_{VIS}(z)$	attenuation coefficient for $E_{VIS}(z)$ between 0 m and depth z	m^{-1}
$\hat{K}_{IR}(z)$	attenuation coefficient for $E_{IR}(z)$ between 0 m and depth z	m^{-1}
$T_{VIS}(z)$	vertical transmittance of $E_{VIS}(z)$, $= E_{VIS}(z)/E_{VIS}(0^-)$	–
$T_{IR}(z)$	vertical transmittance of $E_{IR}(z)$, $= E_{IR}(z)/E_{IR}(0^-)$	–
$T(z)$	vertical transmittance of $E_{SR}(z)$, $= E_{SR}(z)/E_{SR}(0^-)$	–
F_{VIS}	$E_{VIS}(0^-)/E_{SR}(0^-)$	–
IOP	inherent optical properties, mainly referring to the absorption and backscattering coefficients in this paper	m^{-1}
ρ_D	subsurface irradiance reflectance	–
ρ_F	surface Fresnel reflectance	–
θ_a (θ_w)	solar zenith angle above (below) the surface	deg

ficients are kept vertically constant, but horizontally vary with *Jerlov* [1976] water types. Dividing waters into different types is coarse and qualitative, where the attenuation coefficient associated with a water type is a rough estimation. Furthermore, variations of attenuation coefficients within a water type are ignored, and sharp steps between adjacent water types result. In the last decade, advancement in remote sensing of ocean color by satellite has provided fine-scale measurements of optical and biological properties for the world oceans. Therefore models that incorporate these valuable observations better fit the studies of solar heating on global scales.

[5] At present, advanced numerical models [*Gordon et al.*, 1975; *Liu et al.*, 2002; *Mobley*, 1995; *Morel and Gentili*, 1991] have been developed to accurately simulate the subsurface light field with known water properties and boundary conditions. These models, which are excellent for studying the general trend, are impractical for three-dimensional global models because of their computational inefficiency. Simple and efficient models, but without significant loss of accuracy, are required.

[6] On the basis of the strategy of case 1 and case 2 water separation [*Morel and Prieur*, 1977], simple and explicit models have been developed to incorporate satellite-derived chlorophyll concentrations (Chl) into the description of the horizontal and vertical distributions of solar radiation. A model for the spectral diffuse attenuation coefficients ($K_d(\lambda)$) has been specifically developed for the spectrally resolved E_{VIS}, or so-called downwelling spectral irradiance ($E_d(\lambda)$), with values of $K_d(\lambda)$ described as empirical functions of Chl [*Morel*, 1988; *Morel and Maritorena*, 2001]. When Chl values are provided via satellite observations of ocean color [*Carder et al.*, 1999; *Gordon and Morel*, 1983] (see also Ocean color algorithm evaluation, available at http://oceancolor.gsfc.nasa.gov/REPROCESSING/SeaWiFS/R3/), $K_d(\lambda)$ of ocean waters can be evaluated for desired wavelengths. When this information and surface $E_d(\lambda)$ are provided, $E_d(\lambda, z)$ at desired depths can be easily calculated [*Gordon et al.*, 1980], as can $E_{VIS}(z)$, the spectral integration of $E_d(\lambda, z)$ (see Table 1). Note that for the ultraviolet to visible domain, the number of wavelengths can be more than 100 for fine spectral resolution.

[7] Although this wavelength-resolved approach might be required for studies of phytoplankton photosynthesis [*Sathyendranath et al.*, 1989a], it is found "superfluous when dealing with the heating rate" [*Morel and Antoine*, 1994], and computationally expensive for fine-scale three-dimensional modeling of the global oceans. To increase the computation efficiency, without significant loss of accuracy, efforts have been made to simplify the process of modeling the vertical transmittance of E_{VIS}. For this purpose, transmittance of E_{VIS} is usually simplified to a few exponential functions, with a partition factor and an "effective attenuation" coefficient assigned for each term [*Morel and Antoine*, 1994; *Ohlmann and Siegel*, 2000]. Furthermore, these partition factors and attenuation coefficients are expressed as functions of Chl, and/or cloudiness ratios [*Morel and Antoine*, 1994; *Ohlmann and Siegel*, 2000]. Therefore when Chl values and other auxiliary information (such as Sun angle) are available, vertical distribution of E_{VIS} can be quickly provided and efficiently incorporated into physical models.

[8] However, these models or strategies work only for case 1 waters, where all optical properties are determined by Chl alone (with solar zenith angle explicitly or implicitly included) [*International Ocean-Colour Coordinating Group*, 2000; *Morel*, 1988]. Since ocean waters have various combinations of biological and chemical constituents [*Bricaud et al.*, 1981; *Stramski et al.*, 2001], the globally averaged bio-optical relationship could result in big uncertainties for a specific region or a specific time. Fundamentally this is due, first, the optical properties of ocean waters being generally determined by at least three independent variables [*Sathyendranath et al.*, 1989b]: phytoplankton, colored dissolved organic matter (CDOM), and suspended sediments. In many cases knowledge of chlorophyll concentration alone is inadequate to accurately quantify the attenuation coefficients, an optical property. Second,

even for chlorophyll dominated waters, the attenuation coefficient can differ significantly from one time to another or one place to another because of the "package effect" [*Bricaud and Morel*, 1986; *Kirk*, 1994]. These natural variations put significant limitations on the attenuation coefficients calculated on the basis of Chl, and then on the resulting vertical distribution of E_{VIS}.

[9] To avoid such limitations associated with Chl-based models, efforts have also been made to model the vertical transmittance of E_{VIS} as a function of water's optical properties. In an earlier study based on field measurements, *Zaneveld et al.* [1993] modeled the attenuation coefficient of E_{VIS} as a linear function of the diffuse attenuation coefficient at 490 nm. Dividing E_{VIS} of the upper water column into three consecutive layers, separate empirical coefficients were developed for each layer [*Zaneveld et al.*, 1993]. These coefficients, however, remain the same within each layer, which thus cannot represent the steeper than exponential reduction of E_{VIS} in the subsurface layer [*Zaneveld and Spinrad*, 1980]. Later, *Barnard et al.* [1999], on the basis of 30 measurements made around California waters, modeled the attenuation coefficient of E_{VIS} as a polynomial function of depth and absorption coefficient at 490 nm. This empirical model, however, did not consider the effects of scattering and was based on a relatively narrow range of water properties. Its applicability to broader range of waters, especially where scattering by suspended sediments could be important in determining the light field, is unclear [*Barnard et al.*, 1999].

[10] Realizing that water's absorption (a) and backscattering coefficients (b_{b}) can be routinely measured in the field and/or well retrieved from ocean color remote sensing [*Hoge and Lyon*, 1996; *Lee et al.*, 2002; *Loisel et al.*, 2001; *Lyon et al.*, 2004], it would be very useful if a generalized model for the attenuation of $E_{\mathrm{VIS}}(z)$ can be developed that uses values of a and b_{b} as inputs. To reach this goal, we carried out extensive numerical simulations by HydroLight [*Mobley*, 1995; *Mobley et al.*, 2002], and developed a simple model for $\hat{K}_{VIS}(z)$, the vertical attenuation coefficient of E_{VIS}, with a, b_{b}, and z as variables. Combined with the model for $E_{\mathrm{IR}}(z)$, a model with two exponentials is developed for the vertical distribution of $E_{\mathrm{SR}}(z)$. With this model and images of a and b_{b} provided by satellite remote sensing, three-dimensional $E_{\mathrm{SR}}(z)$ in the upper ocean can then be efficiently calculated and implemented into models for heat transfer studies. Separately, $E_{\mathrm{VIS}}(z)$ can be incorporated into photosynthesis models [*Behrenfeld and Falkowski*, 1997] to study primary productivity in the oceans.

2. Vertical Transmittance of E_{IR}

[11] As in the work by *Morel and Antoine* [1994], $E_{\mathrm{SR}}(z)$ is partitioned into two portions: $E_{\mathrm{VIS}}(z)$ (350–700 nm) and $E_{\mathrm{IR}}(z)$ (700–2500 nm):

$$E_{\mathrm{SR}}(z) = E_{\mathrm{VIS}}(z) + E_{\mathrm{IR}}(z). \tag{1}$$

The split is selected at 700 nm instead of 750 nm [*Morel and Antoine*, 1994] to accommodate outputs and models commonly used in physical and biological studies [*Gregg and Carder*, 1990; *Kirk*, 1994; *Morel*, 1978; *Zaneveld et al.*, 1993]. This difference is simply a practical choice, and is not fundamentally different from that of *Morel and Antoine* [1994]. In addition, the split at 700 or 750 nm makes no difference in simulating $E_{\mathrm{SR}}(z)$, as long as it is by the same approach, though a slightly different set of model constants would result.

[12] The vertical distribution of the two components in equation (1) are described by two separate exponential functions,

$$E_{VIS}(z) = E_{VIS}(0^-)e^{-\hat{K}_{VIS}(z)z} \tag{2a}$$

$$E_{IR}(z) = E_{IR}(0^-)e^{-\hat{K}_{IR}(z)z}. \tag{2b}$$

Here $\hat{K}_{VIS}(z)$ and $\hat{K}_{IR}(z)$ in equation (2) are not the values at depth z (so-called local value), but a spatial average between 0 m and z. Also, $\hat{K}_{VIS}(z)$ and $\hat{K}_{IR}(z)$ are spectrally averaged diffuse attenuation coefficients that are weighted by the spectral irradiance in the visible and in the infrared, respectively. Both $\hat{K}_{VIS}$ and $\hat{K}_{IR}$ vary with depth and Sun angle.

[13] Since water's absorption coefficients are extremely large in the infrared domain [*Morel and Antoine*, 1994], $\hat{K}_{IR}$ is considered independent of changes in water constituents. Also, as most of the solar radiation in this domain is absorbed within the layer of top 3 m, *Morel and Antoine* [1994] treated $\hat{K}_{IR}$ independent of z. Here we moved one step further to resolve the vertical variation of $\hat{K}_{IR}$. For this development, we first calculated $\hat{K}_{IR}(z)$ as was done by *Morel and Antoine* [1994],

$$\hat{K}_{IR}(z) = \frac{1}{z}\ln\left(\frac{\int_{700}^{2500} E_d(\lambda, 0^-)d\lambda}{\int_{700}^{2500} E_d(\lambda, 0^-)e^{-a_w(\lambda)z/\cos(\theta_w)}d\lambda}\right), \tag{3}$$

with θ_w the subsurface solar zenith angle. $a_{\mathrm{w}}(\lambda)$ is the absorption coefficient of water in the range of 700–2500 nm, with values taken from *Smith and Baker* [1981] and *Morel and Antoine* [1994]. $E_{\mathrm{d}}(\lambda, 0^-)$ is estimated from MODTRAN 4 with standard marine aerosols (more common for the this study). The effect of aerosol type on the calculated $\hat{K}_{IR}$ is small (~10% for z = 0.5 m and ~7% for z = 2.0 m) even when $E_{\mathrm{d}}(\lambda, 0^-)$ estimated using strong continental aerosols.

[14] From equation (3), values of $\hat{K}_{IR}(z)$ in the layer of 0.01–3.0 m (for z deeper than 3 m, E_{IR} is negligible) are calculated, with Sun angle (θ_a) varying from 0–60° (equivalent to θ_w from 0 to 40°) from zenith. From these $\hat{K}_{IR}(z)$, we found that $\hat{K}_{IR}(z)$ can be described as

$$\hat{K}_{IR}(z, \theta_a) = \left[0.560 + \frac{2.304}{(0.001 + z)^{0.65}}\right](1 + 0.002\theta_a). \tag{4}$$

Figure 1 presents examples of equation (4) modeled $\hat{K}_{IR}(z)$ versus equation (3) calculated $\hat{K}_{IR}(z)$, with an average error of ~3.0%. Clearly, for a change of 2 orders of magnitude of $\hat{K}_{IR}(z)$ in the surface layer, equation (4) represents the vertical variation of $\hat{K}_{IR}(z)$ very well.

[15] Studies [*Pegau et al.*, 1997; *Pegau and Zaneveld*, 1993] have found that values of $a_{\mathrm{w}}(\lambda)$ in the infrared

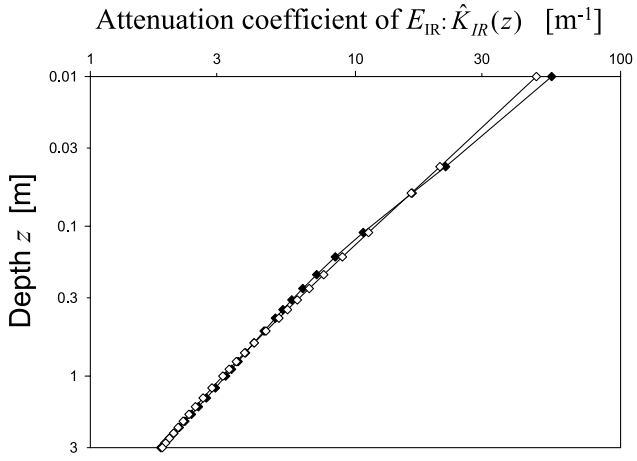

Figure 1. Example of modeled $\hat{K}_{IR}(z)$ (equation (4), open diamonds) compared with calculated $\hat{K}_{IR}(z)$ (equation (3), solid diamonds), with the Sun at 50° from zenith.

domain vary with temperature and salinity, with the temperature effect greater than the salinity effect. This temperature effect is found generally within ~10% of $a_w(\lambda)$ for a temperature range of 0°C to 30°C, and the larger effects only happened at a few wavelengths (such as 750 nm) [see *Pegau et al.*, 1997]. Since $\hat{K}_{IR}(z)$ represents the spectrally integrated attenuation in the wavelength range of 700–2500 nm, the temperature effect at a few wavelengths is considered insignificant to $\hat{K}_{IR}(z)$. Therefore values presented in equation (4) should be applicable to waters with temperature and salinity widely observed in the oceans.

3. Vertical Transmittance of E_{VIS}

[16] For the visible domain, $\hat{K}_{VIS}$ varies not only with depth (the vertical direction), but also with water constituents (the horizontal direction). In order to cope with this three-dimensional change of $\hat{K}_{VIS}$, *Morel and Antoine* [1994] expressed the vertical transmittance of E_{VIS} (represented by T_{VIS}) as

$$T_{VIS}(z) = \frac{E_{VIS}(z)}{E_{VIS}(0^-)} = \sum_{i=1}^{2} v_i e^{-k_i z}. \quad (5)$$

Here v_i and k_i are parameters for T_{VIS} and are constants for different depths. For these multiexponential models, the values of v_i and k_i are further expressed as 5-order polynomial functions of log(Chl) [*Morel and Antoine*, 1994]. Therefore given Chl and z, values of $T_{VIS}(z)$ can be quickly evaluated.

[17] As stated earlier, water's optical properties are generally determined by constituents not limited to Chl, but also by CDOM and suspended sediments [*Sathyendranath et al.*, 1989b]. Furthermore, Chl values derived from remote sensing of ocean color are not as reliable as those of absorption and backscattering coefficients [*Lee et al.*, 2002; *Lyon et al.*, 2004]. To get more accurate vertical distribution of E_{VIS}, an efficient and reliable approach is to estimate $\hat{K}_{VIS}$ (an optical property) directly from water's inherent optical properties (IOP) [*Preisendorfer*, 1976]. A comprehensive model is thus needed to describe the change of $\hat{K}_{VIS}$ for different optical properties and different depths. To develop such a model, concurrent data containing wide range of $\hat{K}_{VIS}(z)$ and the corresponding optical properties are required. In an approach similar to *Ohlmann and Siegel* [2000], we used HydroLight to generate appropriate data sets. From the HydroLight data sets, we developed a model to describe $\hat{K}_{VIS}$ as a function of water's inherent optical properties and depth. Such a model, combined with available optical properties from satellite measurements, can be applied for studies of heat transfer and photosynthesis in global oceans.

4. Numerical Simulations to Obtain $\hat{K}_{VIS}(z)$

[18] As in earlier studies [*Morel and Antoine*, 1994; *Ohlmann and Siegel*, 2000], $\hat{K}_{VIS}(z)$ is first derived from numerically simulated $E_{VIS}(z)$ that corresponds to a wide range of optical properties. As described by *Ohlmann and Siegel* [2000], simulation of $E_d(z, \lambda)$ is carried out by HydroLight. Unlike the simulations of *Ohlmann and Siegel* [2000] where water's IOPs were determined by Chl only, IOPs in our simulations were simulated with varying Chl and independently varying CDOM and suspended sediments, as described by *Lee et al.* [2002] and International Ocean-Colour Coordinating Group/Ocean Colour Algorithm Group (Model, parameters, and approaches used to generate wide range of absorption and backscattering spectra, 2003, available at http://www.ioccg.org/groups/OCAG_data.html). Later, $\hat{K}_{VIS}(z)$ is modeled as a function of total absorption and backscattering coefficients. This way, the concentrations of Chl, CDOM, and sediment are no longer required, as long as accurate total absorption and backscattering coefficients are provided. In natural waters, for the same optical properties, it is common to have different concentrations of Chl, CDOM, and sediments.

[19] For numerical simulations by HydroLight, numerous descriptions can be found in the literature [*Berwald et al.*, 1995; *Lee et al.*, 1998; *Mobley et al.*, 1993, 2002; *Morel and Loisel*, 1998]. The following summarizes the input settings carried out in this study.

[20] 1. The downwelling irradiance at sea surface from the Sun and sky is simulated by the spectral model of *Gregg and Carder* [1990]. A wind speed of 5 m/s is assigned. Sun angles were at 10°, 30°, and 60° from zenith, respectively, with a clear sky.

[21] 2. To determine the light field within the upper water column, HydroLight requires information of water's IOPs. For the attenuation coefficient of downwelling irradiance (the focus of this study), the important IOPs are the total absorption (a) and backscattering coefficients (b_b), as this attenuation is relatively insensitive to the scattering phase function of particles when values of a and b_b are fixed [*Lee et al.*, 2005a]. Chl values ranging from 0.03 to 30.0 mg/m^3 (20 scales with a roughly 50% increasing rate) were used as one free parameter in order to provide a wide range of optical properties. Similar to earlier numerical studies [*Gordon*, 1989; *Kirk*, 1991; *Morel and Loisel*, 1998], all IOPs were kept vertically constant in this study.

[22] 3. Total absorption coefficients were expressed as a sum of the contributions of pure water, phytoplankton

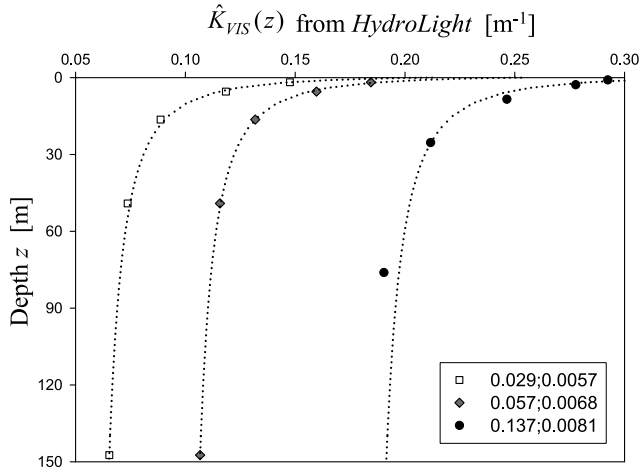

Figure 2. Examples of $\hat{K}_{VIS}(z)$ for different water properties. The numbers in the inset are values of $a(490)$ and $b_b(490)$, respectively. Squares, diamonds, and circles represent $\hat{K}_{VIS}(z)$ from HydroLight simulations, while dotted lines are models from equation (7) (see text for details).

pigments, and CDOM (including detritus). Values of pure water absorption coefficient were taken from *Pope and Fry* [1997], with the pigment absorption coefficient determined by Chl values [*Bricaud et al.*, 1995]. Similar to *Lee et al.* [2002], five different CDOM absorption coefficients for each Chl value were randomly assigned, with the ratio of CDOM absorption to pigment absorption at 440 nm in a range of 0.5 to 5.0 (resulted in a range of 0.017–3.2 m^{-1} for $a(440)$).

[23] 4. Scattering is separated into molecular and nonmolecular (collectively called particle) components [*Gordon and Morel*, 1983; *Morel and Gentili*, 1993; *Sathyendranath et al.*, 2001], with the molecular scattering coefficient taken from *Morel* [1974]. As described in *Lee et al.* [2002], the particle scattering coefficient at 550 nm varied with Chl in a random fashion. The phase function for particle scattering is the average from Petzold's measurements [*Mobley et al.*, 2002]. With these different combinations of Sun angles and water properties, a total of 300 (20 (*Chl*) × 5 (CDOM and particle) × 3 (Sun angles)) HydroLight runs were carried out.

[24] 5. HydroLight simulations were performed for λ in the range of 350–700 nm with a 10-nm spectral resolution. For the same set of optical properties and boundary conditions, sensitivity tests with HydroLight run at a 5-nm resolution showed negligible (<1%) effects on $T_{VIS}(z)$ (not presented).

[25] 6. Five geometric depths (excluding 0 m) were selected for each HydroLight run, with depths spread within and beyond the euphotic zone [*Kirk*, 1994]. Before initiating HydroLight, a preliminary estimation was made to decide the deepest depth (z_d) for each simulation. This z_d is corresponding to $\sim 10^{-3}$ of $E_d(\lambda, 0^-)$, with λ the wavelength with lowest attenuation coefficient (the deepest penetration wavelength) for that spectrum. This 0 to z_d water "slab" is then sliced into five consecutive layers. For the five layers with z_i equal to the position of the bottom of each layer, $E_{VIS}(z_i)/E_{VIS}(0^-)$ span a range of ~ 0–80%. In these HydroLight simulations, corresponding to the different optical properties, the first (z_1) (and last, z_5) depths of the layers ranged from 1.8 (147.4) m for the low absorption case to 0.2 (13.7) m for the high-absorption case.

[26] 7. Bottom reflectance and inelastic scatterings (such as Raman scattering) are excluded as they are beyond the scope of this study. Inelastic scattering makes negligible contributions to heat transfer and photosynthesis in the water column [*Morel and Gentili*, 2004].

[27] Note that the light field is actually determined by the absorption and scattering properties [*Mobley et al.*, 2002], the bio-optical models and the Chl values used in the HydroLight simulations merely provide a wide range of inputs for the numerical simulations [*Kirk*, 1991].

5. Variation of $\hat{K}_{VIS}$ and Its Modeling

[28] From HydroLight simulated $E_{VIS}(z)$, $\hat{K}_{VIS}(z)$ is calculated through

$$\hat{K}_{VIS}(z) = \frac{1}{z}\ln\left(\frac{E_{VIS}(0^-)}{E_{VIS}(z)}\right). \tag{6}$$

Figure 2 presents examples of $\hat{K}_{VIS}(z)$ for a few cases. Not surprisingly, for vertically homogeneous water, $\hat{K}_{VIS}(z)$ still changes a lot (greater than a factor of two) in the subsurface layer. Also, $\hat{K}_{VIS}(z)$ differs significantly for varying water properties. All these variations are the fundamental reasons for the multiple exponentials used to cope with the steep reduction of $E_{VIS}(z)$ below the surface. When a vertically constant value is used to replace $\hat{K}_{VIS}(z)$, it will result in overestimation of E_{VIS} for the near-surface layer and underestimation of E_{VIS} for deeper depths. To accurately describe the vertical distribution of E_{VIS} that is needed for studies of heat transfer and photosynthesis, it is important to know and model the vertical variation of $\hat{K}_{VIS}(z)$.

[29] For each individual $\hat{K}_{VIS}(z)$ profile, we found that it could be well reproduced by a two-parameter model,

$$\hat{K}_{VIS}(IOP, z) = K_1(IOP) + \frac{K_2(IOP)}{(1+z)^{0.5}}. \tag{7}$$

Here K_1 and K_2 are model parameters with K_1 for the asymptotic value at greater depths and K_2 more important to the subsurface $\hat{K}_{VIS}$ value. IOP here represents combinations of different inherent optical properties. K_1 and K_2 in equation (7) do not vary with depth but vary with IOP. The dotted lines in Figure 2 show equation (7) modeled $\hat{K}_{VIS}(z)$ for those examples. Figure 3 presents the result of HydroLight $\hat{K}_{VIS}(z)$ versus equation (7)–modeled $\hat{K}_{VIS}(z)$, for HydroLight simulations with the Sun at 30° from zenith. For the simulated data that $\hat{K}_{VIS}(z)$ ranged from 0.04–1.6 m^{-1}, the average error between HydroLight $\hat{K}_{VIS}(z)$ and equation (7)–modeled $\hat{K}_{VIS}(z)$ is 2.2% (maximum error is 6.4%). Such results clearly demonstrate that equation (7) is adequate to describe the vertical change of $\hat{K}_{VIS}(z)$. Thus the vertical profile of $T_{VIS}(z)$ can be modeled by a single exponential function with two parameters (K_1 and K_2).

[30] For this single exponential term, however, $\hat{K}_{VIS}(z)$ varies with both z and IOP. For global models to incorporate the smooth distributions of water properties obtained from satellite observation of water color, it is necessary to spell

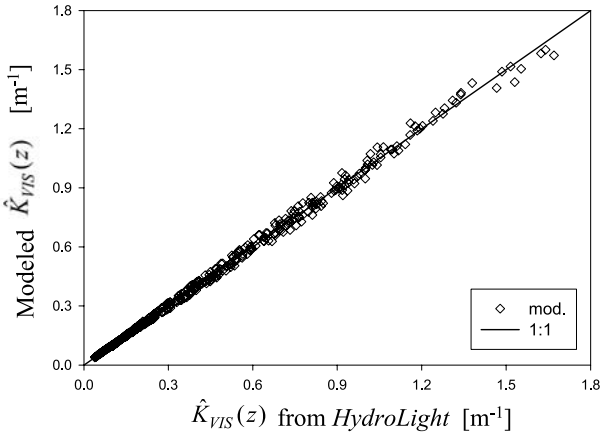

Figure 3. $\hat{K}_{VIS}(z)$ from model (equation (7)) compared with $\hat{K}_{VIS}(z)$ from HydroLight (30° solar zenith angle), indicating that $\hat{K}_{VIS}(z)$ can be well described by equation (7) with two parameters.

out how $K_{1,2}$ vary with water's optical properties, as well as with solar zenith angle. For $\hat{K}_{VIS}(z)$ obtained from HydroLight simulations with the Sun at 30° from zenith, Figure 4 shows the variations of $K_{1,2}$ versus total absorption coefficients at 440 nm and 490 nm. These results show a positive correlation between $K_{1,2}$ and a(440, 490), respectively. Since $K_{1,2}$ also varies with backscattering coefficients (not shown), values of $K_{1,2}$ (and then $\hat{K}_{VIS}(z)$) cannot be well predicted from a(440, 490) alone (see Figure 4). These features, however, suggest that $K_{1,2}$ can be modeled as functions of both total absorption and backscattering coefficients.

[31] Since $K_{1,2}$ are cumulative effects of absorption and scattering in the visible domain, there could be many ways to model $K_{1,2}$ with different combinations of inputs. A simple approach, as suggested by *Zaneveld et al.* [1993] and *Barnard et al.* [1999], is to use absorption and backscattering coefficients at one spectral band, where data from satellite measurements are also available, to model $\hat{K}_{VIS}(z)$. For this approach, we tried to model $K_{1,2}$ using the values at 440 and 490 nm as inputs, respectively, and found using values at 490 nm provided a slightly better result. Therefore empirical models for $K_{1,2}$ are obtained, with

$$K_1(IOP) = \chi_0 + \chi_1(a(490))^{0.5} + \chi_2 b_b(490) \tag{8a}$$

$$K_2(IOP) = \zeta_0 + \zeta_1 a(490) + \zeta_2 b_b(490). \tag{8b}$$

Now, the values of $\chi_{0,1,2}$ and $\varsigma_{0,1,2}$ are independent of both depth and water properties, though they may still vary with solar zenith angle.

[32] To observe the variations of $K_{1,2}$ for different solar zenith angles, values of $K_{1,2}$ from HydroLight simulations with the Sun at 10° and 60° from zenith were analyzed. These results suggested that K_1 only varies slightly for different solar zenith angles, as expected from the asymptotic theory [*Zaneveld*, 1989]. More variations with Sun angles were found for K_2–the parameter important for subsurface solar radiation. On the basis of these $K_{1,2}$ values from HydroLight simulations, equation (8) is expanded to include Sun angle dependence,

$$K_1(IOP, \theta_a) = \left[\chi_0 + \chi_1(a(490))^{0.5} + \chi_2 b_b(490)\right](1 + \alpha_0 \sin(\theta_a)) \tag{9a}$$

$$K_2(IOP, \theta_a) = [\zeta_0 + \zeta_1 a(490) + \zeta_2 b_b(490)](\alpha_1 + \alpha_2 \cos(\theta_a)). \tag{9b}$$

Note that θ_a is the solar zenith angle above the surface. With this model, the final mathematic function for $T_{\mathrm{VIS}}(z)$ became

$$T_{VIS}(IOP, z, \theta_a) = e^{-\hat{K}_{VIS}(IOP, z, \theta_a) z}. \tag{10}$$

By fitting T_{VIS} values from HydroLight simulations with the combination of equations (7), (9), and (10), values of parameters $\chi_{0,1,2}$, $\varsigma_{0,1,2}$, and $\alpha_{0,1,2}$ are derived (provided in Table 2) by least squares curve fitting, as done in earlier studies to derive model parameters [*Morel and Antoine*,

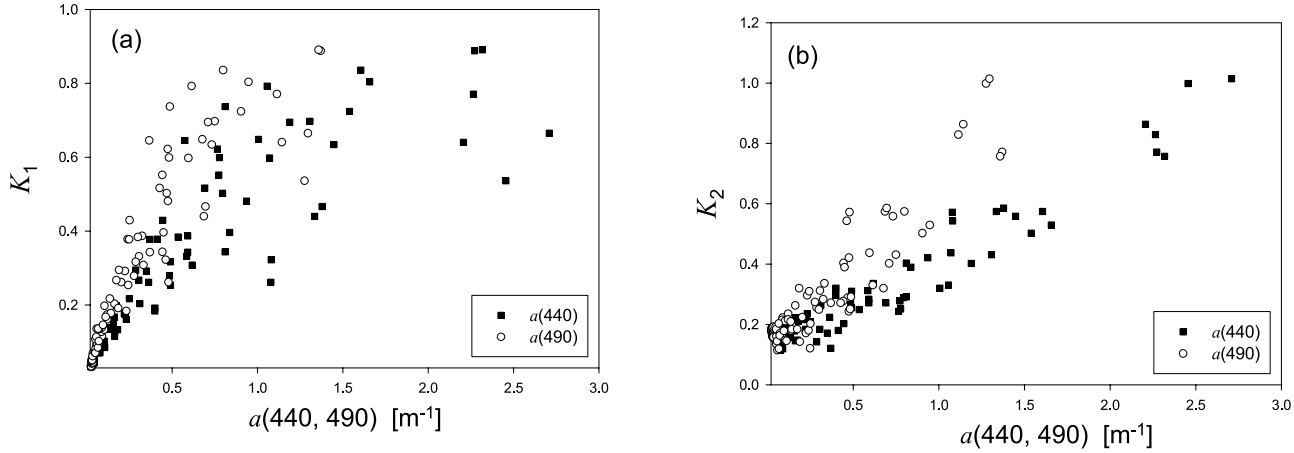

Figure 4. Values of (a) K_1 and (b) K_2, which are model parameters for $\hat{K}_{VIS}(z)$, versus absorption coefficients at 440 nm and 490 nm.

Table 2. Values of the Model Parameters for $\hat{K}_{VIS}(z)$

Parameter	Value
χ_0, m^{-1}	−0.057
χ_1	0.482
χ_2	4.221
ς_0, m^{-1}	0.183
ς_1	0.702
ς_2	−2.567
α_0	0.090
α_1	1.465
α_2	−0.667

1994; *Ohlmann and Siegel*, 2000]. Figure 5 presents equation (10) modeled $T_{\mathrm{VIS}}(IOP, z, \theta_a)$ versus $T_{\mathrm{VIS}}(IOP, z, \theta_a)$ determined from HydroLight simulations. For those T_{VIS} values (limiting to the range of ~0.001 to 0.8), bigger errors happened at $T_{\mathrm{VIS}} < 0.003$, where the effects of E_{VIS} on heat transfer and photosynthesis in the water column are small. For $T_{\mathrm{VIS}} > 0.003$, the average error is ~9%. These results indicate that the simple, optical property-based, model (equation (10)) is adequate for describing the vertical profile of $E_{\mathrm{VIS}}(z)$ for different waters.

6. Improvement Over Chl-Based Models

[33] On the basis of equations (1) and (2), the vertical transmittance (= $E_{\mathrm{SR}}(z)/E_{\mathrm{SR}}(0^-)$) for shortwave solar radiation is

$$T(IOP, z, \theta_a) = F_{VIS} e^{-\hat{K}_{VIS}(IOP, z, \theta_a) z} + (1 - F_{VIS}) e^{-\hat{K}_{IR}(z, \theta_a) z}, \quad (11)$$

with $\hat{K}_{VIS}$ and $\hat{K}_{IR}$ provided by equations (7) and (4), respectively. Here F_{VIS} is the ratio of $E_{\mathrm{VIS}}(0^-)/E_{\mathrm{SR}}(0^-)$, and its value is around 0.424 [*Mobley*, 1994] when the solar radiation is split at 700 nm. Equation (11) is similar to the widely used model of *Paulson and Simpson* [1977, 1981]. The attenuation coefficients in the two models, however, are fundamentally different. The attenuation coefficients in equation (11) vary with depth as suggested from radiative transfer, while they are vertically constant in work by *Paulson and Simpson* [1977].

[34] In order to test the performance of this model and earlier models, a "standard" $T(z)$ data set is generated, which is

$$T(z) = F_{VIS} T_{VIS}(z) + (1 - F_{VIS}) T_{IR}(z), \quad (12)$$

with $T_{\mathrm{VIS}}(z)$ created by HydroLight simulations and $T_{\mathrm{IR}}(z)$ on the basis of equation (3). The HydroLight simulations were run with Chl ranged from 0.03–30 mg/m^3, but with completely different absorption and scattering coefficients as compared to those described in section 4. The depths are fixed at 1, 2, 5, 10, 20, and 50 m, that is, within the commonly observed surface mixed layer. Also, the Sun angle is set at 45° from zenith. Figure 6 shows the values of Chl and $a(490)$ that are used as inputs to these HydroLight simulations and to the $T(z)$ models. The dotted line in Figure 6 represents case 1 $a(490)$ for those Chl values. Clearly, the data set follows the pattern commonly observed in the field [*Gordon and Morel*, 1983; *Morel*, 1988].

[35] There are two earlier models that can provide $T(z)$ for given Chl and z. One is that of *Morel and Antoine* [1994] (MA94 hereafter), where $T(z)$ is described as a sum of three exponentials; another is that of *Ohlmann and Siegel* [2000] (OS00 hereafter), where $T(z)$ is evaluated from a sum of four exponentials. For this standard data set, since values of Chl (so do $a(490)$ and $b_b(490)$) are known, $T(z)$ can be predicted from these models. These $T(z)$ can then be compared to each other, and to the standard data set.

[36] The MA94 model has the same mathematical formulation as equation (12), but the wavelength range is from 300 to 2750 nm and the separation of visible and infrared is at 750 nm. Since solar irradiance at the sea surface in the range of 300–350 nm and 2500–2750 nm are only about 1% of the total irradiance, we applied the model parameters of *Morel and Antoine* [1994] to the standard data set without any change. The split at 750 nm makes the F_{VIS} value different from the F_{VIS} value split at 700 nm, and a value of 0.56 [*Morel and Antoine*, 1994] is used when applied to the MA94 model.

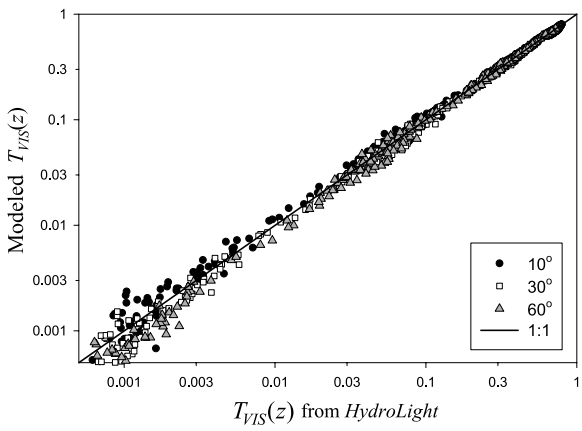

Figure 5. $T_{\mathrm{VIS}}(z)$ from model (equation (10)) compared with $T_{\mathrm{VIS}}(z)$ from HydroLight for three Sun angles.

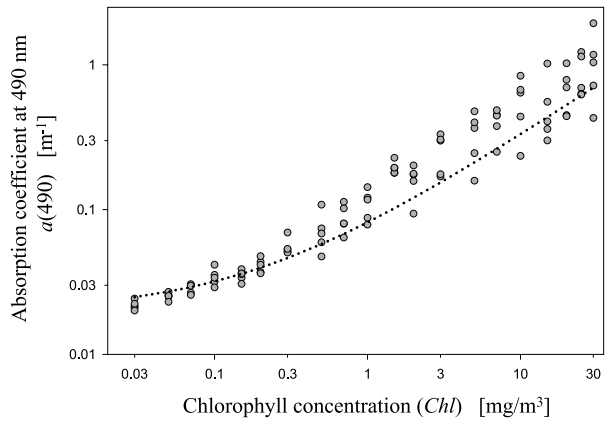

Figure 6. Values of $a(490)$ and *Chl* used in section 6 for model testing. The dotted line is case 1 $a(490)$ for those Chl values, derived on the basis of the $K_d(490)$ model of *Morel* [1988], and $a(490)$ is approximated as 0.9 $K_d(490)$.

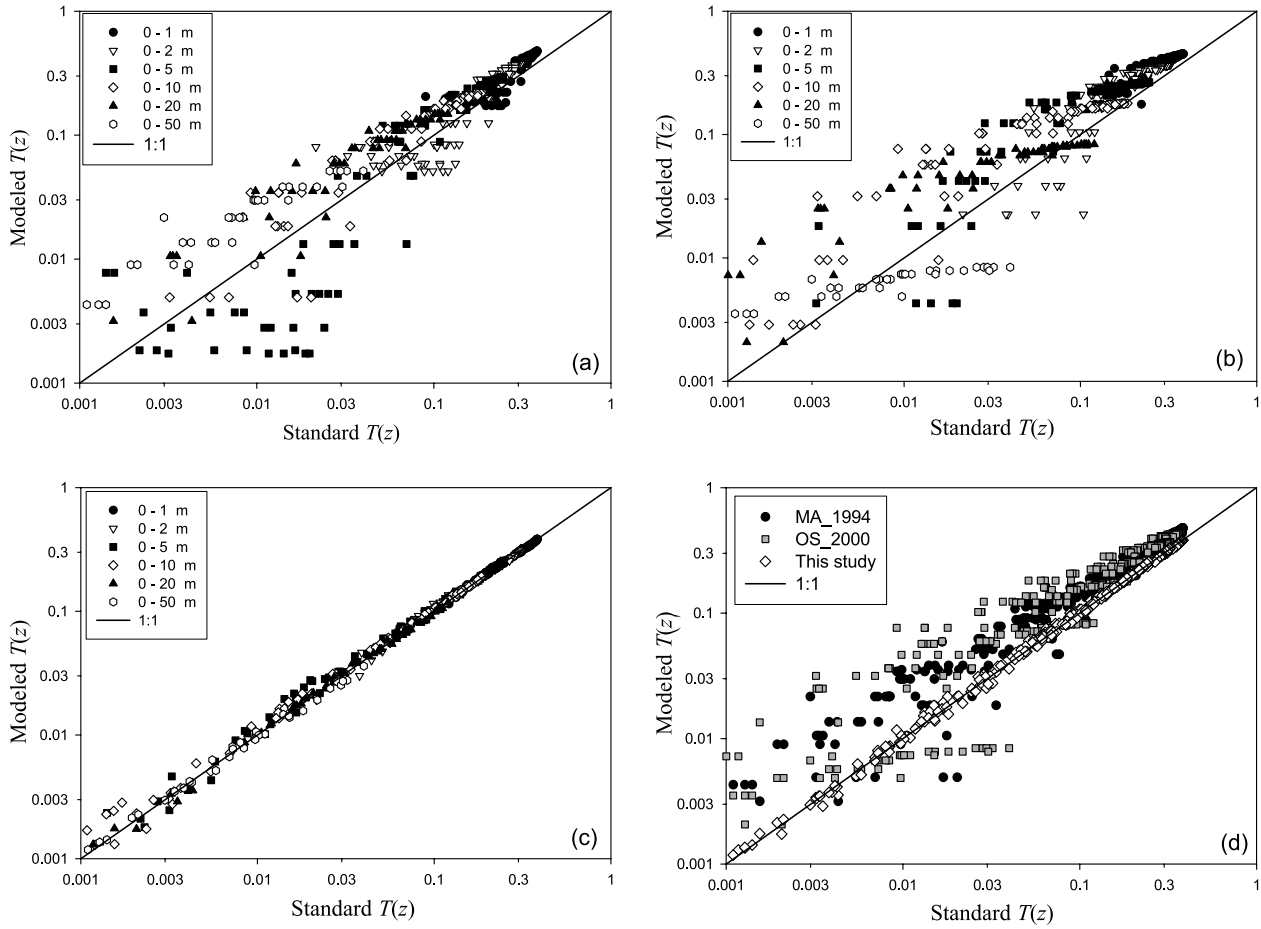

Figure 7. $T(z)$ from models compared with $T(z)$ from the standard data set, where Chl varied from 0.03–30.0 mg/m^3 and z varied from 1 to 50 m: (a) MA94, (b) OS00, (c) the model of this study, and (d) comparison of $T(z)$ of all models for $Chl \leq 3.0$ mg/m^3. Both MA94 and OS00 used Chl value to predict $T(z)$, while model of this study used $a(490)$ and $b_b(490)$ to predict $T(z)$. These Chl, $a(490)$, and $b_b(490)$ values are independent of those discussed in section 4.

[37] The OS00 model (equation (3) of *Ohlmann and Siegel* [2000]) is developed for the ratio of net irradiance flux, that is,

$$T'(z) = \frac{E_{SR}(z) - E_u(z)}{E_{SR}(0^+)}, \tag{13}$$

where $E_u(z)$ is the upwelling irradiance at depth z, and $T'(z)$ is modeled as a sum of four exponentials similar to equation (5). Compared to $T(z)$ defined by *Morel and Antoine* [1994] and in this study, there is

$$T(z) = \frac{T'(z)}{(1 - \rho_F - \rho_D)(1 - \rho_D)}. \tag{14}$$

Here ρ_F is the surface Fresnel reflectance and ρ_D is the irradiance reflectance of water. For a Sun angle of 45°, ρ_F is about 0.03 [*Morel and Antoine*, 1994]. The ρ_D value is generally less than ~0.01 [*Morel and Antoine*, 1994]. We also noticed that the model for $T'(z)$ [*Ohlmann and Siegel*, 2000] was developed for a wavelength range of 250–2500 nm, while the wavelength range in this study is 350–2500 nm. Since solar radiation in the wavelength range shorter than 350 nm is less than 4% of the total at sea surface [*Mobley*, 1994], the influence from this wavelength mismatch on $T(z)$ is very small. Therefore $T(z)$ for the model of *Ohlmann and Siegel* [2000] is approximated as $1.05T'(z)$ on the basis of equation (14) and $T'(z)$ is calculated as in the work by *Ohlmann and Siegel* [2000] for given Chl and z with cloud-free model parameters.

[38] Figure 7 compares model-determined $T(z)$ values to the standard $T(z)$ values for all Chl, with Figure 7a for MA94, Figure 7b for OS00, and Figure 7c for the IOP-based model (equation (11)). Furthermore, Figure 7d compares all modeled $T(z)$ values for Chl ≤ 3.0 mg/m^3, which is usually the upper limit for oceanic waters. All comparisons and analyses are limited to $T(z)$ greater than 0.1% (a total number of 474 left from the 600 "standard" values).

[39] Clearly, for all water properties and depths studied, the $T(z)$ values from the two Chl-based models can differ significantly from the standard $T(z)$ values. Also, although both MA94 and OS00 used the same Chl values to determine $T(z)$, the results from both models are quite different. The R^2 (square of correlation coefficient) values in log transferred domain are 0.79 (slope of 1.18) for MA94

(Figure 7a), and 0.72 (slope of 1.12) for OS00 (Figure 7b). On average, the percentage error for $T(z)$ in log-log scale are ~60% from the two Chl-based models, with MA94 performing slightly better. For Chl $\leq$ 3.0 mg/m^3 (Figure 7d), the performances of the two models are not significantly better. From these Chl-based models, the euphotic zone depth (where $T_{VIS}(z)$ = 1% [*Kirk*, 1994]) can be quite different, and could be significantly deeper or shallower than the actual depth. Note that the approximations made regarding MA94 and OS00 will only cause a small percentage difference in the calculated $T(z)$ compared to their original models.

[40] The $T(z)$ values predicted by the IOP-based model (equation (11)) matched the standard data sets very well for all waters and for all depths (with an average percentage error of ~6% in log-log scale). The R^2 value is 0.99 (slope of 0.99) for data in Figure 7c, also in log transferred domain. Compared to the results from Chl-based models, such results demonstrate the robustness and stability of models on the basis of inherent optical properties. Consequently, the euphotic zone depth can be estimated more accurately. Note that both OS00 and the IOP-based model were developed with data from HydroLight simulations, and that the test data set here is independent of the data used for the development of both models.

[41] Apparently the results presented here were not in favor of Chl-based models. It could be argued that it is not a fair comparison for MA94 and OS00, as in the development of those models Chl values were the only variable used to determine the optical properties of the water. The test data set here, however, deliberately disturbed that picture (see Figure 6), with optical properties determined by Chl and other optically active constituents. So, a mismatch between $T(z)$ from the Chl-based model and $T(z)$ of the test data set is not surprising. This mismatch does not disprove the validation of MA94 and OS00 for water environments where optical properties quantitatively follow the case 1 relationship. More realistically, the results presented here should be viewed as clear evidence that, if water's optical properties do not follow a predefined empirical bio-optical relationship (e.g., the dotted line in Figure 6), the predicted vertical transmittance of E_{VIS} (and E_{SR}) will be subject to big uncertainties. In addition, since optical properties of natural waters are indeed determined by more than the value of Chl [*Sathyendranath et al.*, 1989b; *Stramski et al.*, 2001], this comparison clearly demonstrates the limitations and uncertainties of the Chl-based models, as suggested by *Morel and Antoine* [1994].

[42] For the same wide range of water properties, however, the IOP-based model (equation (11)) provided significantly better results in predicting $T(z)$ for the upper ocean. Since remote sensing of ocean color can provide adequate measurements of water's optical properties for global oceans, clearly the IOP-based model can greatly improve the study of heat transfer and photosynthesis in the upper layer of the global oceans. However, it is necessary to keep in mind that so far this newly developed model and the models of *Morel and Antoine* [1994] and *Ohlmann and Siegel* [2000] are only tested with numerically simulated data. For validation and wide applications, it is essential to test the models with high-quality data obtained from field measurements.

[43] The above compared $T(z)$ values are for a few discrete depths. To reveal the vertical details of $T(z)$ in the subsurface layer, Figure 8 presents examples of $T(z)$ of top 10 m for four commonly observed Chl values in the field. Figure 8 also shows $T(z)$ from the standard data set. Clearly, since *Morel and Antoine* [1994] did not try to resolve the details of $T(z)$ within the top 1 m, larger errors are found for near-surface $T(z)$ in the MA94 model, as pointed out by *Morel and Antoine* [1994]. The models of *Ohlmann and Siegel* [2000] and this study tried to resolve the details of near-surface $T(z)$. In addition, since the attenuation in the infrared domain is dominated by that of pure water, the results between $T(z)$ from OS00 and $T(z)$ from this study show good agreement for the near-surface layer. Note that for $z < 1$ m, changes of water constituents have only minor effects on $T(z)$.

7. Discussion

[44] The $T(z)$ values from the IOP-based model used only absorption and backscattering coefficients at 490 nm; optical properties at other wavelengths were ignored. The robust results from the IOP-based model (see Figures 7 and 8) suggest that knowing the absorption and backscattering coefficient at 490 nm is adequate for estimation of the vertical transmittance of E_{VIS} and E_{SR}, as implied in earlier studies [*Barnard et al.*, 1999; *Zaneveld et al.*, 1993]. This is somewhat surprising, because for studies such as the estimation of primary production detailed spectral information is important [*Sathyendranath et al.*, 1989a]. The reason for this relaxed requirement in spectral information is that the focus of this study is the spectrally integrated solar radiation that is available for water heating. There could be quite different absorption coefficients at 350 or 410 nm for the same absorption coefficient at 490 nm [*Lee et al.*, 2005b], and these differences will result in different irradiance for those wavelengths at a specific depth. These irradiances, however, are only a small portion of the total solar radiation, and the decrease of irradiance at one wavelength may be compensated by an increase at another wavelength at that depth, so the sum of the irradiance of all wavelengths (which gives E_{VIS} and E_{SR}) may not vary much. Such a scenario is not true for depths below the euphotic zone where irradiance is eventually concentrated to a narrow band; but the contribution of solar radiation at such a spectral band and at such depths is small compared to the absorbed solar energy in the upper water column.

[45] The results presented here show significant improvements in modeling of the vertical distribution of E_{VIS} and E_{SR} in the upper ocean by utilization of IOPs. Such an approach is adequate for satellite remote sensing of ocean color and in environments where water's optical properties are well measured. However, if Chl value is the only available parameter for a water environment, since there are wide uncertainties in estimating its IOPs, we expect no significant difference in estimated $T(z)$ from either IOP-based model or MA94 or OS00. It is recognized that the accuracy of IOPs (a(490), for instance) derived from ocean color to the best can be within ~10% [*Lee et al.*, 2002]. This error will be propagated to the calculated $\hat{K}_{VIS}(z)$ and then $T_{VIS}(z)$. However, since $\hat{K}_{VIS}(z)$ is a spectrally averaged value with a big portion determined by the large absorption

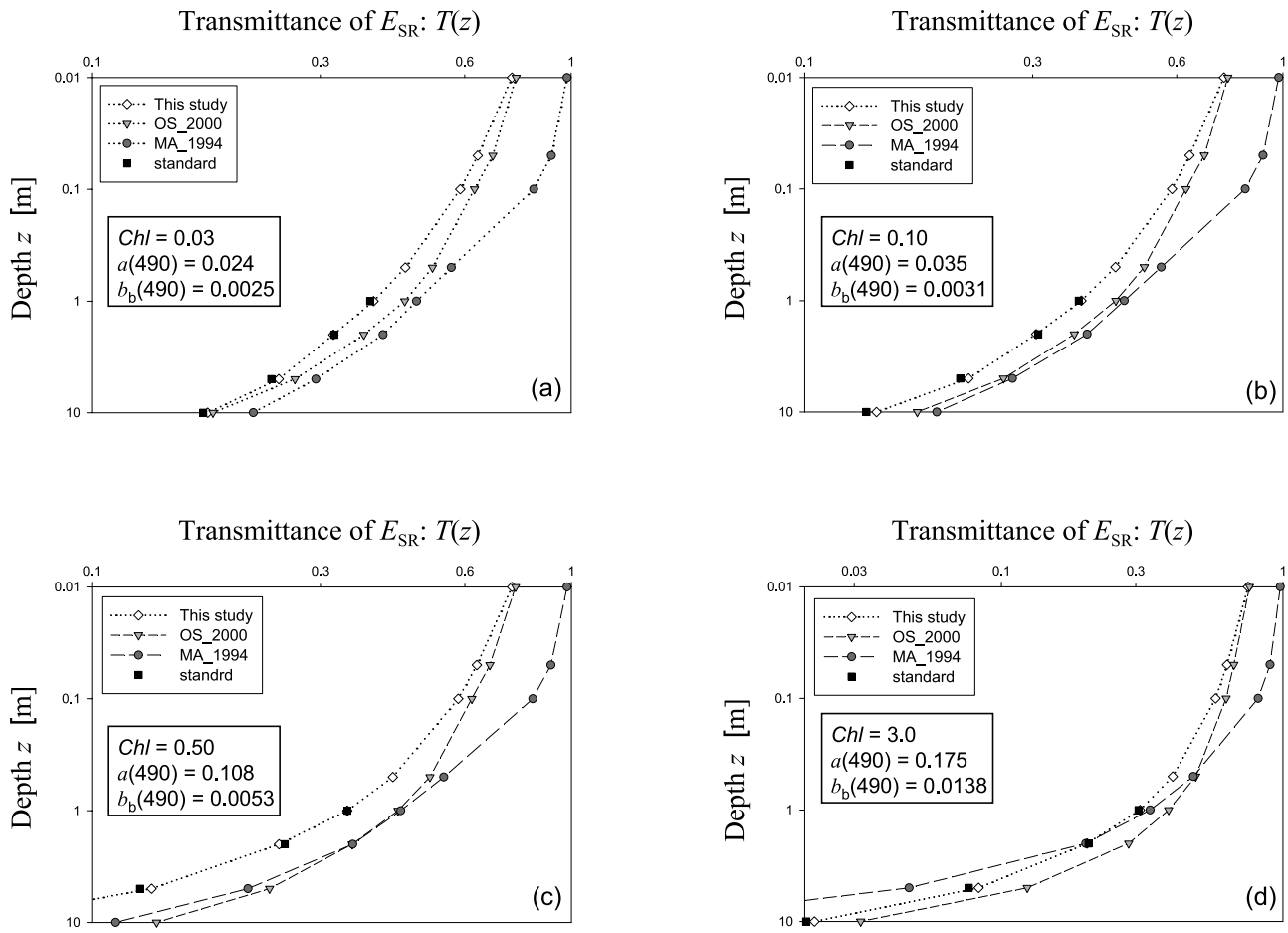

Figure 8. Examples of $T(z)$ for the top 10 m, with $T(z)$ calculated by three models and from the standard data set. Values of Chl, $a(490)$, and $b_b(490)$ are provided in the insets.

coefficients of $a_w(\lambda)$ in the red wavelengths, only a fraction of errors in IOPs will be transferred to $K_{VIS}(z)$.

[46] It is necessary to point out that the model developed here has primarily demonstrated the strategy, concept, and advantages of modeling the vertical transmittance of E_{VIS} and E_{SR} using inherent optical properties. The work here presented a model with the major variables such as IOPs and Sun angle incorporated, and the model is for clear-sky conditions with marine aerosols and a well-mixed surface layer [*Mueller and Lange*, 1989]. When the sky is cloudy, reduction of the total downwelling irradiance and the ratio of the visible portion (F_{VIS}) need to be adjusted accordingly [*Behrenfeld and Falkowski*, 1997; *Ohlmann and Siegel*, 2000]. However, a recent study [*Bartlett et al.*, 1998] pointed out that clouds have only a small spectral effect on surface E_{VIS}, which suggests that model parameters developed in this study could be applicable to cloudy conditions, though a slight adjustment for θ_a (or subsurface solar zenith angle as in work by *Sathyendranath and Platt* [1988]) is necessary. Similarly, when the subsurface light field is more diffuse as a result of capillary waves [*Zaneveld et al.*, 2001], an effective θ_a might also be required. However, the effects of slightly incorrect θ_a on the attenuation of E_{VIS} are much smaller than that of incorrect absorption and backscattering coefficients.

[47] One should take caution when applying the newly developed model to depths that are below the well-mixed surface layer, especially if the optical properties at those depths are significantly different from those in the mixed layer. For such conditions, the evaluation of downwelling irradiance at those depths will be changed, and the properties retrieved from observed ocean color might also be affected [*Gordon and Clark*, 1980; *Sathyendranath and Platt*, 1989; *Zaneveld et al.*, 1998]. A critical hurdle in remote sensing is the lack of instantaneous knowledge of the vertical distribution of the optical properties when a satellite sensor makes measurements. Historical data may provide a general guidance about the vertical distributions, but those measurements are insufficient and the vertical distributions vary spatially and temporally. A method to adequately provide the details of the vertical distribution of the optical or biogeochemical properties of a water body is needed. Combining measurements from satellite sensors with outputs from dynamic oceanography models [*Chai et al.*, 2002; *McGillicuddy et al.*, 1995] may provide useful alternatives to overcome the limitations of significantly stratified upper water column.

8. Conclusions

[48] In this study, an innovative model is developed for describing the vertical transmittance of solar radiation in the upper layer of the oceans. Similar to *Morel and Antoine* [1994], our study explicitly partitioned the solar radiation

into two portions: one for the visible domain (E_{VIS}, 350–700 nm), and the other for the infrared domain (E_{IR}, 700–2500 nm). For the two portions, two exponential functions are used separately to describe their vertical transmittance. For each exponential term, an attenuation coefficient is assigned. For E_{IR}, its attenuation coefficient ($\hat{K}_{IR}(z)$) is modeled as a function of z and solar zenith angle. For E_{VIS}, its attenuation coefficient ($\hat{K}_{VIS}(z)$) is modeled as a function of depth, solar zenith angle, and water's optical properties, after extensive numerical simulations using HydroLight.

[49] Compared with earlier Chl-based models, the model developed here has fewer empirical parameters and provides robust and stable results in describing the vertical distribution of the visible portion or the full spectrum of solar radiation in the subsurface layer. Since the model requires $a(490)$ and $b_b(490)$ as inputs, accurate retrieval of these two optical properties from satellite observations of ocean color is required. When these properties are available for world oceans, the model can be used to provide efficient evaluation of $E_{VIS}(z)$ and $E_{SR}(z)$ in the well mixed upper water column, which in turn can be incorporated into physical models to study heat transfer [e.g., *Kara et al.*, 2005]. Also, after consideration of the average cosine [*Sathyendranath and Platt*, 1988], $E_{VIS}(z)$ can be easily converted to photosynthetic available radiation (PAR) and incorporated into models for estimating primary production of the water column. In addition, the $\hat{K}_{VIS}(z)$ model provides an easy and reliable tool to predict the light level at desired depths from satellite IOPs, needed to plan the C^{14} incubation for in situ measurements of primary production [*Barnard et al.*, 1999].

[50] **Acknowledgments.** Support for this study was provided by the Office of Naval Research (P.E. 61153N and N0001405WX20623). The authors thank Robert F. Chen for assistance in MODTRAN calculation and Heather Melton Penta for editorial contribution, and the authors are very grateful to Curtis Mobley for providing HydroLight code and assistance. Comments and suggestions from two reviewers are greatly appreciated.

References

Barnard, A. H., J. R. V. Zaneveld, W. S. Pegau, J. L. Mueller, H. Maske, R. Lara-Lara, S. Alvarez-Borrego, R. Cervantes-Duarte, and E. Valdez-Holguin (1999), The determination of PAR levels from absorption coefficient profiles at 490 nm, *Cienc. Mar.*, *25*(4), 487–507.

Bartlett, J. S., A. M. Ciotti, R. F. Davis, and J. J. Cullen (1998), The spectral effects of clouds on solar irradiance, *J. Geophys. Res.*, *103*, 31,017–31,031.

Behrenfeld, M. J., and P. G. Falkowski (1997), A consumer's guide to phytoplankton primary productivity models, *Limnol. Oceanogr.*, *42*, 1479–1491.

Berwald, J., D. Stramski, C. D. Mobley, and D. A. Kiefer (1995), Influences of absorption and scattering on vertical changes in the average cosine of the underwater light field, *Limnol. Oceanogr.*, *40*, 1347–1357.

Bricaud, A., and A. Morel (1986), Light attenuation and scattering by phytoplanktonic cells: A theoretical modeling, *Appl. Opt.*, *25*, 571–580.

Bricaud, A., A. Morel, and L. Prieur (1981), Absorption by dissolved organic matter of the sea (yellow substance) in the UV and visible domains, *Limnol. Oceanogr.*, *26*, 43–53.

Bricaud, A., M. Babin, A. Morel, and H. Claustre (1995), Variability in the chlorophyll-specific absorption coefficients of natural phytoplankton: Analysis and parameterization, *J. Geophys. Res.*, *100*, 13,321–13,332.

Carder, K. L., F. R. Chen, Z. P. Lee, S. K. Hawes, and D. Kamykowski (1999), Semianalytic Moderate-Resolution Imaging Spectrometer algorithms for chlorophyll a and absorption with bio-optical domains based on nitrate-depletion temperatures, *J. Geophys. Res.*, *104*, 5403–5422.

Chai, F., R. C. Dugdale, T.-H. Peng, F. P. Wilkerson, and R. T. Barber (2002), One-dimensional ecosystem model of the equatorial Pacific upwelling system, part I: Model development and silicon and nitrogen cycle, *Deep Sea Res., Part II*, *49*, 2713–2745.

Chang, G. C., and T. D. Dickey (2004), Coastal ocean optical influences on solar transmission and radiant heating rate, *J. Geophys. Res.*, *109*, C01020, doi:10.1029/2003JC001821.

Gordon, H. R. (1989), Can the Lambert-Beer law be applied to the diffuse attenuation coefficient of ocean water?, *Limnol. Oceanogr.*, *34*, 1389–1409.

Gordon, H. R., and D. K. Clark (1980), Remote sensing optical properties of a stratified ocean: An improved interpretation, *Appl. Opt.*, *19*, 3428–3430.

Gordon, H. R., and A. Morel (1983), *Remote Assessment of Ocean Color for Interpretation of Satellite Visible Imagery: A Review*, 44 pp., Springer, New York.

Gordon, H. R., O. B. Brown, and M. M. Jacobs (1975), Computed relationship between the inherent and apparent optical properties of a flat homogeneous ocean, *Appl. Opt.*, *14*, 417–427.

Gordon, H. R., R. C. Smith, and J. R. V. Zaneveld (1980), Introduction to ocean optics, in *Proc. SPIE Soc. Opt. Eng.*, *208*, 1–43.

Gregg, W. W., and K. L. Carder (1990), A simple spectral solar irradiance model for cloudless maritime atmospheres, *Limnol. Oceanogr.*, *35*, 1657–1675.

Hoge, F. E., and P. E. Lyon (1996), Satellite retrieval of inherent optical properties by linear matrix inversion of oceanic radiance models: An analysis of model and radiance measurement errors, *J. Geophys. Res.*, *101*, 16,631–16,648.

International Ocean-Colour Coordinating Group (2000), Remote sensing of ocean colour in coastal, and other optically-complex, waters, *Rep. 3*, edited by S. Sathyendranath, 140 pp., Dartmouth, Nova Scotia, Canada.

Jerlov, N. G. (1976), *Marine Optics*, Elsevier, New York.

Kara, A. B., A. J. Wallcraft, and H. E. Hurlburt (2005), Sea surface temperature sensitivity to water turbidity from simulations of the turbid Black Sea using HYCOM, *J. Phys. Oceanogr.*, *35*, 33–54.

Kirk, J. T. O. (1988), Solar heating of water bodies as influenced by their inherent optical properties, *J. Geophys. Res.*, *93*, 10,897–10,908.

Kirk, J. T. O. (1991), Volume scattering function, average cosines, and the underwater light field, *Limnol. Oceanogr.*, *36*, 455–467.

Kirk, J. T. O. (1994), *Light and Photosynthesis in Aquatic Ecosystems*, Cambridge Univ. Press, New York.

Lee, Z. P., K. L. Carder, C. D. Mobley, R. G. Steward, and J. S. Patch (1998), Hyperspectral remote sensing for shallow waters. 1. A semianalytical model, *Appl. Opt.*, *37*, 6329–6338.

Lee, Z. P., K. L. Carder, and R. Arnone (2002), Deriving inherent optical properties from water color: A multi-band quasi-analytical algorithm for optically deep waters, *Appl. Opt.*, *41*, 5755–5772.

Lee, Z. P., K. P. Du, and R. Arnone (2005a), A model for the diffuse attenuation coefficient of downwelling irradiance, *J. Geophys. Res.*, *110*, C02016, doi:10.1029/2004JC002275.

Lee, Z. P., W. J. Rhea, R. Arnone, and W. Goode (2005b), Absorption coefficients of marine waters: Expanding multi-band information to hyperspectral data, *IEEE Trans. Geosci. Remote Sens.*, *43*(1), 118–124.

Lewis, M. R., M. Carr, G. Feldman, W. Esaias, and C. McMclain (1990), Influence of penetrating solar radiation on the heat budget of the equatorial Pacific Ocean, *Nature*, *347*, 543–545.

Liu, C.-C., R. Miller, K. L. Carder, and Z. P. Lee (2002), Estimating the underwater light field from remote sensing, in *Ocean Optics XVI* [CD-ROM], edited by S. Ackleson, Off. of Naval Res. Arlington, Va.

Loisel, H., D. Stramski, B. G. Mitchell, F. Fell, V. Fournier-Sicre, B. Lemasle, and M. Babin (2001), Comparison of the ocean inherent optical properties obtained from measurements and inverse modeling, *Appl. Opt.*, *40*, 2384–2397.

Lyon, P. E., F. E. Hoge, C. W. Wright, R. N. Swift, and J. K. Yungel (2004), Chlorophyll biomass in the global oceans: Satellite retrieval using inherent optical properties, *Appl. Opt.*, *43*, 5886–5892.

McClain, C., K. Arrigo, K.-S. Tai, and D. Turk (1996), Observations and simulations of physical and biological process at ocean weather station P, 1951–1980, *J. Geophys. Res.*, *101*, 3697–3713.

McGillicuddy, D. J., J. J. McCarthy, and A. R. Robinson (1995), Coupled physical and biological modeling of the spring bloom in the North Atlantic I: Model formulation and one dimensional bloom processes, *Deep Sea Res., Part I*, *42*, 1313–1357.

Mobley, C. D. (1994), *Light and Water: Radiative Transfer in Natural Waters*, Elsevier, New York.

Mobley, C. D. (1995), Hydrolight 3.0 users' guide, SRI Int., Menlo Park, Calif.

Mobley, C. D., B. Gentili, H. R. Gordon, Z. Jin, G. W. Kattawar, A. Morel, P. Reinersman, K. Stamnes, and R. H. Stavn (1993), Comparison of numerical models for computing underwater light fields, *Appl. Opt.*, *32*, 7484–7504.

Mobley, C. D., L. K. Sundman, and E. Boss (2002), Phase function effects on oceanic light fields, *Appl. Opt.*, *41*, 1035–1050.

Morel, A. (1974), Optical properties of pure water and pure sea water, in *Optical Aspects of Oceanography*, edited by N. G. Jerlov and E. S. Nielsen, pp. 1–24, Elsevier, New York.

Morel, A. (1978), Available, usable, and stored radiant energy in relation to marine photosynthesis, *Deep Sea Res.*, *25*, 673–688.

Morel, A. (1988), Optical modeling of the upper ocean in relation to its biogenous matter content (case I waters), *J. Geophys. Res.*, *93*, 10,749–10,768.

Morel, A., and D. Antoine (1994), Heating rate within the upper ocean in relation to its bio-optical state, *J. Phys. Oceanogr.*, *24*, 1652–1665.

Morel, A., and B. Gentili (1991), Diffuse reflectance of oceanic waters: Its dependence on Sun angle as influenced by the molecular scattering contribution, *Appl. Opt.*, *30*, 4427–4438.

Morel, A., and B. Gentili (1993), Diffuse reflectance of oceanic waters. II. Bidirectional aspects, *Appl. Opt.*, *32*, 6864–6879.

Morel, A., and B. Gentili (2004), Radiation transport within oceanic (case 1) water, *J. Geophys. Res.*, *109*, C06008, doi:10.1029/2003JC002259.

Morel, A., and H. Loisel (1998), Apparent optical properties of oceanic water: Dependence on the molecular scattering contribution, *Appl. Opt.*, *37*, 4765–4776.

Morel, A., and S. Maritorena (2001), Bio-optical properties of oceanic waters: A reappraisal, *J. Geophys. Res.*, *106*, 7163–7180.

Morel, A., and L. Prieur (1977), Analysis of variations in ocean color, *Limnol. Oceanogr.*, *22*, 709–722.

Mueller, J. L., and R. E. Lange (1989), Bio-optical provinces of the northeast Pacific Ocean: A provisional analysis, *Limnol. Oceanogr.*, *34*, 1572–1586.

Mueller, R. W., et al. (2004), Rethinking satellite-based solar irradiance modelling: The SOLIS clear-sky module, *Remote Sens. Environ.*, *91*, 160–174.

Ohlmann, J. C., and D. Siegel (2000), Ocean radiant heating. Part II: Parameterizing solar radiation transmission through the upper ocean, *J. Phys. Oceanogr.*, *30*, 1849–1865.

Ohlmann, J. C., D. A. Siegel, and C. D. Mobley (2000), Ocean radiant heating. part I: Optical influences, *J. Phys. Oceanogr.*, *30*, 1833–1848.

Paulson, C. A., and J. J. Simpson (1977), Irradiance measurements in the upper ocean, *J. Phys. Oceanogr.*, *7*, 953–956.

Paulson, C. A., and J. J. Simpson (1981), The temperature difference across the cool skin of the ocean, *J. Geophys. Res.*, *86*, 11,044–11,054.

Pegau, W. S., and J. R. V. Zaneveld (1993), Temperature-dependent absorption of water in the red and near-infrared portions of the spectrum, *Limnol. Oceanogr.*, *38*, 188–192.

Pegau, W. S., D. Gray, and J. R. V. Zaneveld (1997), Absorption and attenuation of visible and near-infrared light in water: Dependence on temperature and salinity, *Appl. Opt.*, *36*, 6035–6046.

Pope, R., and E. Fry (1997), Absorption spectrum (380–700 nm) of pure waters: II. Integrating cavity measurements, *Appl. Opt.*, *36*, 8710–8723.

Preisendorfer, R. W. (1976), *Hydrologic Optics*, vol. 1, *Introduction*, Natl. Tech. Inf. Serv., Springfield, Va.

Sathyendranath, S., and T. Platt (1988), The spectral irradiance field at the surface and in the interior of the ocean: A model for applications in oceanography and remote sensing, *J. Geophys. Res.*, *93*, 9270–9280.

Sathyendranath, S., and T. Platt (1989), Remote sensing of ocean chlorophyll: Consequence of nonuniform pigment profile, *Appl. Opt.*, *28*, 490–495.

Sathyendranath, S., T. Platt, C. M. Caverhill, R. E. Warnock, and M. R. Lewis (1989a), Remote sensing of oceanic primary production: Computations using a spectral model, *Deep Sea Res., Part A*, *36*, 431–453.

Sathyendranath, S., L. Prieur, and A. Morel (1989b), A three-component model of ocean colour and its application to remote sensing of phytoplankton pigments in coastal waters, *Int. J. Remote Sens.*, *10*, 1373–1394.

Sathyendranath, S., G. Cota, V. Stuart, M. Maass, and T. Platt (2001), Remote sensing of phytoplankton pigments: A comparison of empirical and theoretical approaches, *Int. J. Remote Sens.*, *22*, 249–273.

Schneider, E. K., and Z. Zhu (1998), Sensitivity of the simulated annual cycle of sea surface temperature in the Equatorial Pacific to sunlight penetration, *J. Clim.*, *11*, 1932–1950.

Siegel, D., J. C. Ohlmann, L. Washburn, R. R. Bidigare, C. T. Nosse, E. Fields, and Y. Zhou (1995), Solar radiation, phytoplankton pigments and radiant heating of the equatorial Pacific warm pool, *J. Geophys. Res.*, *100*, 4885–4891.

Simpson, J. J., and T. D. Dickey (1981), Alternative parameterizations of downward irradiance and their dynamic significance, *J. Phys. Oceanogr.*, *11*, 876–882.

Smith, R. C., and K. S. Baker (1981), Optical properties of the clearest natural waters, *Appl. Opt.*, *20*, 177–184.

Stramski, D., A. Bricaud, and A. Morel (2001), Modeling the inherent optical properties of the ocean based on the detailed composition of the planktonic community, *Appl. Opt.*, *40*, 2929–2945.

Zaneveld, J. R. V. (1989), An asymptotic closure theory for irradiance in the sea and its inversion to obtain the inherent optical properties, *Limnol. Oceanogr.*, *34*, 1442–1452.

Zaneveld, J. R. V., and R. W. Spinrad (1980), An arc tangent model of irradiance in the sea, *J. Geophys. Res.*, *85*, 4919–4922.

Zaneveld, J. R. V., J. C. Kitchen, and H. Pak (1981), The influence of optical water type on the heating rate of a constant depth mixed layer, *J. Geophys. Res.*, *86*, 6426–6428.

Zaneveld, J. R. V., J. C. Kitchen, and J. L. Mueller (1993), Vertical structure of productivity and its vertical integration as derived from remotely sensed observations, *Limnol. Oceanogr.*, *38*, 1384–1393.

Zaneveld, J. R. V., A. H. Barnard, W. S. Pegau, and E. Boss (1998), An investigation into the appropriate depth average of remotely sensed optical parameters, in *Ocean Optics XIV* [CD-ROM], edited by S. Ackleson and J. Campbell, Off. of Naval Res. Arlington, Va.

Zaneveld, J. R. V., E. Boss, and P. A. Hwang (2001), The influence of coherent waves on the remotely sensed reflectance, *Opt. Express*, *9*(6), 260–266.

R. Arnone, Z. Lee, and B. Penta, Naval Research Lab, Code 7333, Stennis Space Center, MS 39529, USA. (zplee@nrlssc.navy.mil)

K. Du, State Key Laboratory of Remote Sensing Science, Research Center for Remote Sensing and GIS, School of Geography, Beijing Normal University, Beijing, 100875, China.

S. Liew, Center for Remote Imaging, Sensing and Processing, National University of Singapore, Lower Kent Ridge Road, Singapore 119260.